

# Autonomous frequency locking for zero-offset microcomb

Ming Li,<sup>1,2,\*</sup> Feng-Yan Yang,<sup>1,2,\*</sup> Juanjuan Lu,<sup>3</sup> Guang-Can Guo,<sup>1,2</sup> and Chang-Ling Zou<sup>1,2,†</sup>

<sup>1</sup>CAS Key Laboratory of Quantum Information, University of Science and Technology of China, Hefei 230026, P. R. China.

<sup>2</sup>CAS Center For Excellence in Quantum Information and Quantum Physics,

University of Science and Technology of China, Hefei, Anhui 230026, P. R. China.

<sup>3</sup>School of Information Science and Technology, ShanghaiTech University, 201210 Shanghai, China.

(Dated: March 6, 2024)

The stabilization of optical frequency comb conventionally relies on active electronic feedback loops and stable frequency references. Here, we propose a new approach for autonomous frequency locking (AFL) to generate a zero-offset frequency comb based on cooperative nonlinear optical processes in a microcavity. In a simplified few-mode system, AFL enables the concept of fractional harmonic generation as a zero-offset multi-laser reference for measuring the carrier envelope offset frequency ( $f_{\text{ceo}}$ ) of frequency combs spanning less than one octave, such as  $1/3$  octave. Combining with Kerr comb generation in a microcavity, AFL is further applied to directly generate zero- $f_{\text{ceo}}$  soliton comb that is robust against fluctuations in pump laser and cavity resonances. Numerical simulations validate the AFL scheme, showing good agreement with analytical prediction of the locking condition. This work presents a new pathway for exploring novel frequency locking mechanisms and technologies using integrated photonic devices, and also appeals further investigations of cooperative nonlinear optics processes in microcavities.

## I. INTRODUCTION

Integrated photonic devices have greatly promoted the development of nonlinear optics in the last decades [1–5], benefiting from enhanced nonlinear interaction and flexible dispersion engineering in wavelength-scale structures [6–10]. These devices bring the nonlinear optics into a cascaded regime, where multiple nonlinear processes that involve multiple modes occur simultaneously in a single configuration [11]. The cooperation of different nonlinear processes has attracted research interests in exploring new physics, such as the interference of  $\chi^{(2)}$  and  $\chi^{(3)}$  processes [12–16], the competition between Raman/Brillouin scattering and Kerr processes [17–21], and the synthetic high-order nonlinearity [22]. It has also encouraged tremendous applications in optical frequency comb [23–30], quantum frequency conversion [12, 13, 31–34], and quantum optics sources [35–38].

Compared with bulk and fiber nonlinear optics, the ability to harness complex nonlinear processes on photonic chip platform provides new opportunity to control the spatio-temporal property of optical fields. For example, traditional electronic control and feedback functions could potentially be realized all-optically with higher stability and shorter latency based on enhanced nonlinearity in microcavity, which is vital for the coherence of lasers. In particular, when incorporating competing nonlinear processes with optical gain such as optical parametric oscillation (OPO), phase transition phenomena (e. g. frequency locking and optical self-organization) may arise [39–43]. For example, in a pure  $\chi^{(3)}$  cavity, optical field can be self-organized to stable temporal pulses or frequency-locked comb employing cascaded four-wave mixing (FWM) among optical modes, known as the dissipative Kerr soliton (DKS) [44–46]. Nonetheless, ensuring the stability of the repetition frequency ( $f_{\text{rep}}$ ) and carrier-envelope offset frequency ( $f_{\text{ceo}}$ ) remains imperative to counter the impact of environmental and laser fluctuations in practical scenario [47–52].

This necessitates a stable external reference and high-speed active feedback.

In this Letter, we propose a new mechanism for autonomous all-optical frequency locking in a single microresonator employing the cooperative nonlinear optical interactions between a network of optical modes. First, in presence of second-harmonic generation (SHG), we demonstrate that the  $\chi^{(3)}$  OPO laser frequencies can be precisely locked to the  $\frac{2}{3}$  and  $\frac{4}{3}$  of the pump frequency, manifesting the capabilities of fractional-harmonic generation. The self-locked lasers, as a zero-offset frequency reference, are robust against cavity and pump laser fluctuations, which makes them well-suited for measuring the  $f_{\text{ceo}}$  of combs as well as severing as seed for producing zero- $f_{\text{ceo}}$  combs. Second, we generalize the mechanism to a microresonator supporting DKS and demonstrate an autonomous frequency-locked microcomb with zero  $f_{\text{ceo}}$ . Our work provides insights for investigating self-frequency locking protocols based on cooperative nonlinear optics in multimode microresonators on a chip and developing novel photonic devices with engineered nonlinear optical functions.

## II. ZERO-OFFSET FREQUENCY REFERENCE

As a unique feature of integrated nonlinear photonic devices, different kinds of nonlinearity link multiple photonic modes at different wavelength bands [Fig. 1(a)]. Such nonlinear optics network offers all-optical feedback mechanism to stabilize the frequency of lasers using only  $\chi^{(2)}$  and  $\chi^{(3)}$  nonlinearities. To generate an equally spaced frequency frame with zero offset, we consider the model that involves the  $\chi^{(3)}$  degenerate OPO and second-harmonic generation (SHG). These processes as individual components have become the kernel element of many integrated nonlinear photonic devices with ultra-low power consumption [53–56]. For the degenerate OPO, it arises from the parametric interaction between three

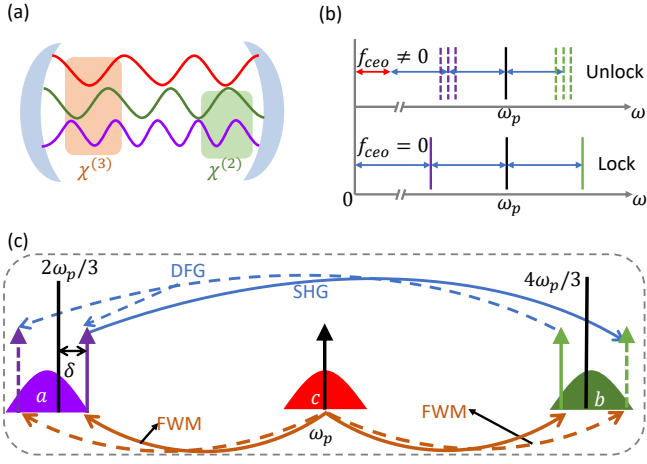


**Fig 1.** Principle of zero-offset frequency reference. (a) Illustration of a resonator for cascaded FWM ( $\chi^{(2)}$ ) and SHG ( $\chi^{(2)}$ ) processes. (b) Frequency tones generated by FWM without (upper) and with (lower) SHG. (c) Closed-cascaded nonlinear optical network for autonomously locked zero-offset reference.  $\omega_p$ : frequency of the pump laser,  $\omega_{i,s}$ : frequency of OPO laser, FWM: four-wave mixing, SHG: second-harmonic generation, DFG: difference frequency generation.

photonic modes, following the Hamiltonian

$$H_{\text{FWM}} = \sum_j \omega_j j^\dagger j + g_3 (abc^{\dagger 2} + a^\dagger b^\dagger c^2), \quad (1)$$

where  $j \in \{a, b, c\}$  ( $j^\dagger$ ) represents the annihilation (creation) operator of the mode,  $g_3$  is the nonlinear coupling rate and  $\omega_j$  is the corresponding frequency.

In absence of the  $\chi^{(2)}$  process, the OPO is driven by an input laser  $\omega_p$  on mode  $c$  with a strength  $\varepsilon_p$ , which starts new laser frequencies  $\omega_{i,s}$  when operation above the OPO threshold, with  $\omega_i + \omega_s = 2\omega_p$ . It forms the elementary process in Kerr comb formation and generates equally-spaced frequency frame [Fig. 1(b)]. By choosing  $\omega_{a,b}$  to be  $\frac{2}{3}\omega_p$  and  $\frac{4}{3}\omega_p$ , it is expected the pump, signal and idler lasers form a three-line comb with zero frequency offset. However, the mode resonances can be hardly designed to these values, and environment noise and pump fluctuations also shift these resonances. The lasing frequency  $\omega_s$  with respect to the mode resonance  $\omega_a$  ( $\delta = \omega_i - \omega_a$ ) is [57]

$$\delta = \frac{\Delta_b \kappa_a - \Delta_a \kappa_b}{\kappa_a + \kappa_b}, \quad (2)$$

is usually sensitive to fluctuations of resonance and dissipation, where  $\Delta_a = \omega_a - \frac{2}{3}\omega_p$ ,  $\Delta_b = \omega_b - \frac{4}{3}\omega_p$  and  $\kappa_a, \kappa_b$  are dissipation rates of mode  $a, b$ . Consequently, the three-line comb has a non-zero as well as fluctuating offset frequency  $f_{ceo}$ , which cannot be regarded as reliable frequency reference, shown by dashed lines in Fig. 1(b). Here the offset frequency is defined as the minimum positive value  $f_{ceo} = \omega_s - n f_{rep}$  for  $n \in \mathbb{Z}$ .

This fluctuation can be eliminated by introducing frequency conversion between mode  $a$  and  $b$  to form a closed loop,

which imposes an additional constraint  $\omega_s = f(\omega_i)$  on the  $\omega_{s,i}$ . Together with  $\omega_i + \omega_s = 2\omega_p$ , the OPO lasing frequencies are uniquely determined by  $\omega_p$  and frequency conversion if the system allows a steady state. The physical mechanism of the autonomous locking network is revealed by a practical model shown in Fig. 1(c). Here the SHG

$$H_{\text{SHG}} = g_2 (a^{\dagger 2} b + a^2 b^\dagger), \quad (3)$$

between mode  $a, b$  is introduced concurrently with the OPO, where  $g_2$  is the nonlinear coupling rate of SHG. This interaction takes place when the mode  $a, b$  are chosen around  $2\omega_p/3$  and  $4\omega_p/3$ . Such octave spanning OPO has already been demonstrated in integrated nonlinear platforms by special dispersion engineering [53, 58, 59]. According to Eq. (2), the lasing frequency [purple solid arrow in Fig. 1(c)] is not necessarily equal to  $2\omega_p/3$  (black bar) with  $\Delta = \omega_i - 2\omega_p/3 = \Delta_a + \delta$ , which depends on the mode detuning and dissipation. Then the  $\chi^{(2)}$  interaction in Eq. (3) will generate additional sidebands (Dashed arrows) located symmetrically around the pump. As a result, the beating of these laser tones in each mode leads to periodic oscillation of the field intensity instead of a steady state solution.

However, the  $\chi^{(2)}$ -assisted sideband-pair (Dashed arrows) also participates into the interaction in Eq. (1), which stimulates new FWM and competes with the original FWM (Solid arrows). Meanwhile, the stimulated FWM also promotes the original OPO through the  $\chi^{(2)}$  conversion. The mutually reinforcing and competitive relationship means a steady state solution is only permitted when  $\delta = 0$ . By solving the dynamics of the cascaded nonlinear process [57] we find the condition

$$9g_2^4 \alpha^4 - 4(\Delta_a - \Delta_b)^2 \kappa^2 + 4g_2^2 \alpha^2 (9\Delta_a \Delta_b + \kappa^2) \geq 0, \quad (4)$$

is necessary for the steady state existence, where  $\alpha$  is the photon number amplitude of mode  $a$ . Similar condition applies to mode  $b$ . For small detuning  $\Delta_{a,b} \ll \kappa$ , the condition reduces to

$$g_2^2 \alpha^2 \geq (\Delta_a - \Delta_b)^2. \quad (5)$$

In this case, the laser frequencies in mode  $a, b$  are autonomously locked to the fractional harmonics  $2\omega_p/3, 4\omega_p/3$  of the pump laser. Consequently, the three-line comb is autonomously locked to zero offset and remains robust against fluctuations in the pump or environment, in contrary to the unlocked OPO case [Fig. 1(b)].

The autonomous locking is verified numerically by analyzing the power spectral dynamics of the field when the pump laser frequency is scanned, as shown in Fig. 2(a). As pump laser scans into the resonance of mode  $c$ , the cavity field intensity increases and the  $\chi^{(2)}$  interaction is gradually enhanced. Above a threshold, the parametric laser field jumps from an unlocked multi-tone state to a locked single-tone state with frequency equals exactly to  $2/3\omega_p$ , which confirms the mechanism of frequency locking. To quantify the robustness of locking against parameter variations, we define the locking

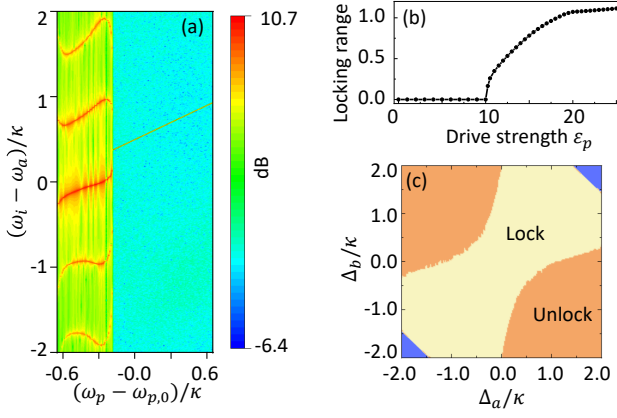


**Fig. 2.** Power spectral dynamics during autonomous frequency locking. (a) Dynamics of intracavity power spectrum of mode  $a$  as the pump laser  $\omega_p$  scanning across the resonance. The OPO laser frequency  $\omega_i$  has a single peak at the fractional harmonic frequency  $2/3\omega_p$  after the system is locked. Initial detuning  $\Delta_a = -0.5\kappa$ ,  $\Delta_b = 0.3\kappa$ ,  $\kappa_a = \kappa_b = \kappa$ . (b) Relationship between the drive strength  $\varepsilon_p^2$  normalized to  $10^6\kappa$  and the locking range. (c) Phase diagram of the system. The system operates below the OPO threshold inside the blue areas. In the calculation, experimental feasible parameters  $g_3/\kappa = 10^{-7}$  and  $g_2/\kappa = 10^{-3}$  are chosen.

range as the maximum detuning  $\Delta_b$  that can support the locked state by fixing  $\Delta_a = 0$ . It can be inferred from Eq. (5) that higher  $g_2$  and stronger field intensity  $\alpha$  leads to larger locking range, where  $\alpha$  can be increased by increasing pump strength  $\varepsilon_p$ , as confirmed by Fig. 2(b). Figure 2(c) shows the phase diagram of the system for a fixed pump power  $P_{in}/\hbar\omega_p = 10^7\kappa_a$ , with the stability being justified by the Routh-Hurwitz criterion [60]. The locking phase (brown, Fig. 2(d)) lies in the area where  $\Delta_a$  and  $\Delta_b$  have comparable values, which is consistent with Eq. (5).

Autonomous locking enables a novel type of nonlinear frequency conversion process, i.e., fractional harmonic generation, which is distinct from conventional integer harmonic generation. For optical frequency comb with  $f_n = f_{ceo} + n f_{rep}$ , measurement and stabilization of repetition rate  $f_{rep}$  and offset frequency  $f_{ceo}$  is essential for its precision applications. The zero-offset reference enabled by fractional harmonic generation simplifies the measurement of  $f_{ceo}$  by alleviating the need for an octave-spanning comb [49, 61–63], as required in the traditional  $f$ - $2f$  self-referencing scheme. For the example in Fig. 1(c), the frequency-locked lasers  $\omega_p$  and  $\frac{4}{3}\omega_p$  can be used to beat with nearby comb lines  $f_{m_1}$ ,  $f_{m_2}$  and extracting  $f_{ceo}$  by  $f_{ceo} = (3m_2 - 4m_1)f_{rep} \mp 3\Delta_1 \pm 4\Delta_2$ , with  $\Delta_1$ ,  $\Delta_2$  being the corresponding beating frequencies. In this scheme, a comb with only  $\frac{1}{3}$  octave bandwidth is required, which is equivalent to  $3f$ - $4f$  scheme in self-referencing. Moreover, based on our autonomous locking network,  $\frac{7}{6}\omega_p$  can be generated by a degenerate FWM from  $\omega_p$  and  $\frac{4}{3}\omega_p$ , which further enables the measurement of  $f_{ceo}$  for a  $\frac{1}{7}$  octave comb. Such function corresponds to  $7f$ - $8f$  self-referencing, which is very challenging

due to the involving higher-order harmonics [61]. Based on the zero-offset reference, a zero- $f_{ceo}$  comb is also possible by generating other equally-spaced comb lines using FWM, or injection locking the frequency of a Kerr comb.

The mechanism of autonomous locking can be generalized to other closed cascaded nonlinear networks involving competing nonlinear processes, such as  $\chi^{(2)}$  OPO or laser process. The SHG can be also replaced by sum-frequency generation, electro-optics or other nonlinear processes with the modified function  $\omega_s = f(\omega_i, \omega_{ex})$ . Generally, the FC can be driven by nonzero external frequency  $\omega_{ex}$ , thus the OPO laser frequencies  $\omega_{i,s}$  are determined not only by  $\omega_p$  but also  $\omega_{ex}$ , which offers new possibility for the laser frequency stabilization in noisy environment without active feedback components.

### III. ZERO- $f_{ceo}$ SOLITON COMB

The pump laser  $\omega_p$  and OPO lasers  $\frac{2}{3}\omega_p, \frac{4}{3}\omega_p$  essentially form a three-line comb with  $f_{ceo} = 0$  and  $f_{rep} = \frac{1}{3}\omega_p$ . By extending the three-mode model to multi modes, the multi-mode microcomb is also expected to be locked autonomously with  $f_{ceo} = 0$ . Here we integrate  $\chi^{(2)}$  interaction with Kerr comb generation, where comb line  $f_n$  is frequency-doubled to be  $2f_n$ , as shown in the dashed purple line in Fig. 3(a). Likewise, difference-frequency generation (DFG) from comb lines  $f_{2n}$  and  $f_n$  results in  $f_{2n} - f_n$  (red dashed line in Fig. 3(a)). These sidebands compete with and promote the original comb generation, eventually leading to a steady state solution in which all frequency components within a specific cavity mode merge into a single frequency tone, i.e.,  $f_{2n} = 2f_n$ . Consequently, a soliton state with  $f_{ceo}$  locked precisely at zero is created. During such process,  $f_{rep}$  satisfies the demands of both FWM and SHG in a self-adaptive manner. This autonomous locking mechanism contains only optical processes, eliminating the need for a complicated electronic feedback loop that is typically required in active stabilization scheme.

Using the typical parameters in LiNbO<sub>3</sub> microring [53, 57], we numerically confirmed the existence of zero- $f_{ceo}$  frequency comb. Starting with a soliton state with initial carrier-envelope-offset frequency  $f_0 = \omega_p - n_p f_{rep} = 2\kappa$  ( $n_p$  is the comb line indice of the pump laser), we first modify integrated dispersion  $D_{int}$  at targeted fundamental (F) and second harmonic (SH) modes to boost their photon number for enhancing the effective  $\chi^{(2)}$  coupling, as Fig. 3(b) shows. Subsequently,  $\chi^{(2)}$  interaction is introduced with the varying  $g_2$  values [57]. By analyzing the time evolution of SH mode intensity, we can ascertain whether  $f_{ceo}$  is locked to zero. This is because if  $f_{ceo}$  deviates from zero, multiple frequency tone will be generated in a single mode and results in oscillation of field intensity. With a relative weak coupling rate  $g_2 = 1.2$  MHz, the photon number in SH mode keeps oscillating, indicating an unlocked state [blue curve in Fig. 3(c)]. By increasing  $g_2$  to 2.4 MHz, the constant photon number in SH mode after evolution indicates a steady soliton state with zero  $f_{ceo}$  [orange curve in Fig. 3(c)]. This verifies that proper  $\chi^{(2)}$

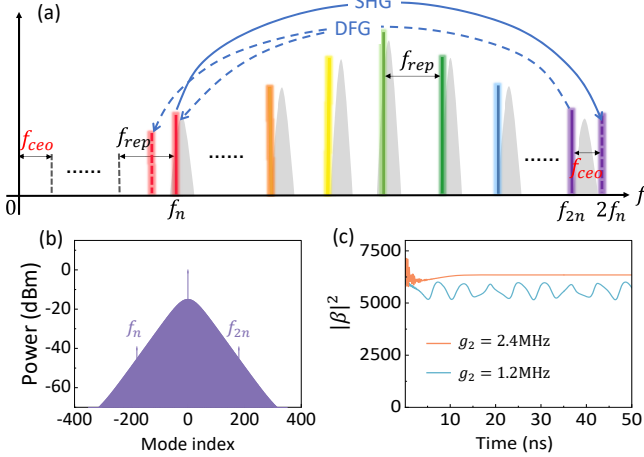


**Fig 3.** Autonomously locked zero- $f_{ceo}$  microcomb. (a) Illustration of  $\chi^{(2)}$  nonlinear processes in zero- $f_{ceo}$  microcomb generation. (b) The optical spectrum of Kerr soliton with initial carrier-envelope-offset frequency  $f_0$  equals  $2\kappa$ . Modes with relative index -180 and 180 are selected as fundamental and SH mode to participate in further  $\chi^{(2)}$  interaction, respectively. Parameter: pump frequency  $\omega_p = 193.55$  THz, mode number  $m_p = 540$ , second-order dispersion coefficient  $D_2 = 0.67$  MHz, cavity mode amplitude loss rate  $\kappa = 94.89$  MHz. (c) The SH mode field dynamics of the locked (orange) and unlocked (blue) microcomb.

interaction indeed modifies the soliton state, and adjusts  $f_{rep}$  automatically to align with an integer division of pump laser frequency. As the feedback loop is entirely optical, it takes approximately 10 ns [Fig. 3(c)] to achieve a stable locked state, significantly quicker than a feedback loop including external electronics.

To demonstrate the robustness of self-locking mechanism, we investigate the locking range of this scheme. Here we define the locking range as the maximum initial carrier-envelope-offset frequency  $f_0$  that allows autonomous locking by  $\chi^{(2)}$  interaction. Since  $f_0 = \omega_p - n_p f_{rep}$ , it reflects robustness against drifting of the pump laser and cavity free spectral range (FSR). As indicated by Eq. (5) of the three-mode model, the locking range for soliton comb should be proportional to  $\chi^{(2)}$  nonlinear coupling rate  $g_2$ . Figure 4(a) shows the dependence of locking range on the  $g_2$  values when keeping photon number fixed for all comb lines in the initial soliton state. A good linear relationship is revealed and is consistent with the simplified three-mode model. In our simulation, locking range of  $2\kappa = 189.78$  MHz corresponds to a tolerable pump drifting of 189.78 MHz and cavity FSR drifting of 0.35 MHz. The larger the locking range, the stronger robustness against pump and FSR drift.

Though the simplified three-mode model gives an intuitive understanding for  $f_{ceo}$ -locking of the comb state, the complex nonlinear dynamics of multimode comb state prevents a simple analytical expression of the autonomous locking condition similar to Eq. (5). First, different from the simple three-mode

model where the photon numbers increase with pump power, photon numbers in soliton state are clamped due to the balance between cavity dispersion and Kerr nonlinearity [64], thus the locking range is greatly limited. Second, it is difficult to change the frequencies of hundreds of comb lines with only two-mode nonlinear interaction. Third, the  $\chi^{(2)}$  interaction strength is limited for not destroying steady soliton state [24, 65]. Therefore, we numerically study the locking dynamics in the weak coupling regime, where the photon numbers involved in the SHG are mainly determined by the initial soliton state itself and the influence of SHG is treated as perturbation.

The locking range should depend on both the F and SH field amplitudes, denoted by  $\alpha$  and  $\beta$ . Considering that the contribution of SHG to  $\beta$  (DFG to  $\alpha$ ) is proportional to  $g_2 \alpha^2$  ( $2g_2 \alpha^* \beta$ ), the locking range is conjectured to be proportional to  $\sqrt{|\alpha|^2 + 2|\alpha\beta|}$ . We numerically simulate how the locking range changes with the photon number  $|\alpha|^2$  in fundamental mode while keeping  $|\beta|^2$  fixed, whose result [red circles in Fig. 4(b)] is well-fitted by the formula  $f_0/\kappa = \sqrt{p_1|\alpha|^2 + p_2\alpha}$  and thereby justifies the scaling relationship between the locking range and photon number  $|\alpha|^2$ . Fitting of locking range versus photon number  $|\beta|^2$  in SH mode with formula  $f_0/\kappa = \sqrt{p_3|\beta| + p_4}$  further consolidates the scaling relationship, as shown in Fig. 4(c).

Based on the above analysis, we define a figure of merit as

$$\text{FOM} = \frac{g_2}{f_0} \cdot \sqrt{|\alpha|^2 + 2|\alpha\beta|}, \quad (6)$$

to judge whether a comb state can be locked. Figure 4(d) plots the value of FOM for soliton samples with different photon numbers  $|\alpha|^2$  and  $|\beta|^2$ , while their initial  $f_0$  was fixed to be  $3\kappa$ . These soliton samples are evolved with  $g_2 = 2.4$  MHz, and the ones that finally have  $f_{ceo}$  locked are located between the blue and gray dots in the FOM phase diagram. The solid line represents the analytical results for  $\text{FOM} = 1.56$  as defined by Eq. 6, which coincides well with the boundary (blue dots) between unlocked and locked area for small photon numbers. The locking boundary deviation in the large- $|\beta|^2$ -regime is mainly attributed to the strong  $\chi^{(2)}$  interaction beyond the perturbation regime. The further increasing photon number in both F and SH modes disturbs the system more, leading to the collapse of soliton state and giving the upper boundary of locking region, as presented in the upper right corner in Fig. 4(d).

#### IV. DISCUSSION AND CONCLUSION

The application of the autonomous locking mechanism would be greatly extended if it can be realized with pure  $\chi^{(3)}$  nonlinearity, which is widely adopted for comb generation in leading platforms such as silicon nitride (SiN) [10, 66]. It has already been experimentally demonstrated that the effective SHG can be realized in  $\chi^{(3)}$  material such as, silicon [67] and



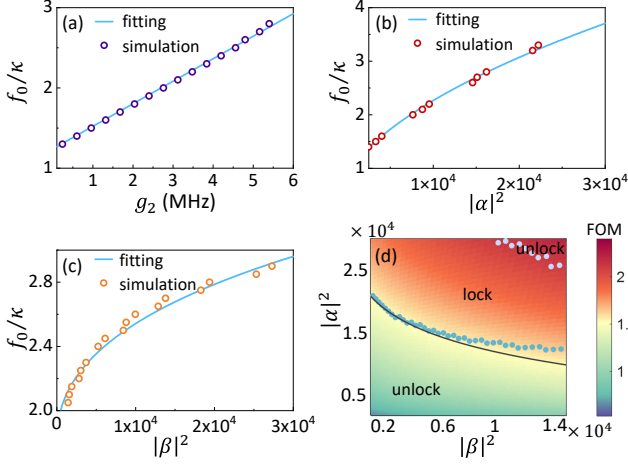


**Fig 4.** Locking range of zero- $f_{\text{cco}}$  microcomb. (a) Relationship between the SHG coupling rate  $g_2$  and the locking range  $f_0/\kappa$ . The locking boundary is fitted using linear equation  $f_0/\kappa = p_1 g_2 + q_1$  with  $p_1 = 0.2807, q_1 = 1.2411$ . (b) Relationship between locking range and fundamental photon number  $|\alpha|^2$  when keeping  $|\beta|^2 \simeq 3000, g_2 = 2.4 \text{ MHz}$ . The locking range is fitted with  $f_0/\kappa = \sqrt{p_2 |\alpha|^2 + q_2}$  with  $p_2 = 4.2994 \times 10^{-4}, q_2 = 0.8368$ . (c) Relationship between locking range and fundamental photon number  $|\beta|^2$  when keeping  $|\alpha|^2 \simeq 10000, g_2 = 2.4 \text{ MHz}$ . The locking range is fitted with  $f_0/\kappa = \sqrt{p_3 |\beta|^2 + q_3}$  with  $p_3 = 0.0314, q_3 = 3.3189$ . (d) The phase diagram of FOM. The comb can be  $f_{\text{cco}}$ -locked in the region between the blue and gray dots. The solid line shows the lower boundary for  $f_{\text{cco}}$ -locking defined by  $\text{FOM}=1.56$ .

SiN [68] by a biased static electric field. Such schemes synthesize an effective second-order susceptibility  $\chi_{\text{eff}}^{(2)} = E \cdot \chi^{(3)}$  that is proportional to the amplitude of the biased electric field  $E$ . The zero- $f_{\text{cco}}$  soliton comb can be obtained following the same procedure as the  $\chi^{(2)}$  case. More generally, the biased electric field can be also time-dependent, i.e., a microwave field with frequency  $\omega_{\text{ex}}$  then the modified steady state of the soliton comb should fulfill  $2(f_{\text{cco}} + n f_{\text{rep}}) \pm \omega_{\text{ex}} = f_{\text{cco}} + n f_{\text{rep}}$ , resulting in a locked  $f_{\text{cco}}$  with tunable frequency  $\omega_{\text{ex}}$  or  $f_{\text{rep}} - \omega_{\text{ex}}$ .

In conclusion, we have proposed a mechanism to autonomously lock the frequency of OPO lasers based on the closed cascaded nonlinear optical network. The autonomous locking enables high-order fractional harmonic generation, which not only enriches nonlinear frequency conversion, but also generates frequency-locked zero-offset reference allowing for feasible measurement and stabilization of the  $f_{\text{cco}}$  of narrow frequency combs. By further applying the locking mechanism to Kerr soliton generation, the  $f_{\text{cco}}$  can be autonomously locked to zero, which is robust against the fluctuations of pump laser frequency and cavity resonances. We also propose an approximate analytical expression for the autonomous locking condition, which is verified by the numerical simulations. The autonomous locking mechanism is universal for closed cascaded nonlinear optical network and is

also applicable to  $\chi^{(3)}$  nonlinear optical platforms.

This work was funded by the National Key R&D Program (Grant No. 2021YFF0603701), the National Natural Science Foundation of China (Grants No. 12374361, No. 12293053, No. 62305214 and 92265210). It was also supported by the Fundamental Research Funds for the Central Universities, the USTC Research Funds of the Double First-Class Initiative. The numerical calculations in this paper have been done on the supercomputing system in the Supercomputing Center of the University of Science and Technology of China. This work was partially carried out at the USTC Center for Micro and Nanoscale Research and Fabrication.

\* These authors contribute equally to this work.

† [clzou321@ustc.edu.cn](mailto:clzou321@ustc.edu.cn)

- [1] A. Boes, L. Chang, C. Langrock, M. Yu, M. Zhang, Q. Lin, M. Lončar, M. Fejer, J. Bowers, and A. Mitchell, Lithium niobate photonics: Unlocking the electromagnetic spectrum, *Science* **379**, eabj4396 (2023).
- [2] D. J. Wilson, K. Schneider, S. Hönl, M. Anderson, Y. Baumgartner, L. Czornomaz, T. J. Kippenberg, and P. Seidler, Integrated gallium phosphide nonlinear photonics, *Nature Photonics* **14**, 57 (2020).
- [3] S. M. Hendrickson, A. C. Foster, R. M. Camacho, and B. D. Clader, Integrated nonlinear photonics: emerging applications and ongoing challenges, *JOSA B* **31**, 3193 (2014).
- [4] H. Shu, L. Chang, Y. Tao, B. Shen, W. Xie, M. Jin, A. Nether-ton, Z. Tao, X. Zhang, R. Chen *et al.*, Microcomb-driven silicon photonic systems, *Nature* **605**, 457 (2022).
- [5] J. Liu, F. Bo, L. Chang, C.-H. Dong, X. Ou, B. Regan, X. Shen, Q. Song, B. Yao, W. Zhang *et al.*, Emerging material platforms for integrated microcavity photonics, *Science China Physics, Mechanics & Astronomy* **65**, 104201 (2022).
- [6] D. V. Strelakov, C. Marquardt, A. B. Matsko, H. G. Schwefel, and G. Leuchs, Nonlinear and quantum optics with whispering gallery resonators, *Journal of Optics* **18**, 123002 (2016).
- [7] S. Kim, K. Han, C. Wang, J. A. Jaramillo-Villegas, X. Xue, C. Bao, Y. Xuan, D. E. Leaird, A. M. Weiner, and M. Qi, Dispersion engineering and frequency comb generation in thin silicon nitride concentric microresonators, *Nature Communications* **8**, 372 (2017).
- [8] X. Xue, Y. Xuan, Y. Liu, P.-H. Wang, S. Chen, J. Wang, D. E. Leaird, M. Qi, and A. M. Weiner, Mode-locked dark pulse kerr combs in normal-dispersion microresonators, *Nature Photonics* **9**, 594 (2015).
- [9] M. H. Anderson, A. Tikan, A. Tusnin, J. Riemensberger, A. Davydova, R. N. Wang, and T. J. Kippenberg, Dissipative solitons and switching waves in dispersion-modulated kerr cavities, *Physical Review X* **13**, 011040 (2023).
- [10] J. Liu, G. Huang, R. N. Wang, J. He, A. S. Raja, T. Liu, N. J. Engelsen, and T. J. Kippenberg, High-yield, wafer-scale fabrication of ultralow-loss, dispersion-engineered silicon nitride photonic circuits, *Nature communications* **12**, 2236 (2021).
- [11] L. Zhang, X. Wu, Z. Hao, R. Ma, F. Gao, F. Bo, G. Zhang, and J. Xu, Second-harmonic and cascaded third-harmonic generation in generalized quasiperiodic poled lithium niobate waveguides, *Optics Letters* **48**, 1906 (2023).
- [12] M. Li, C.-L. Zou, C.-H. Dong, X.-F. Ren, and D.-X. Dai, Enhancement of second-harmonic generation based on the cas-

- caded second- and third-order nonlinear processes in a multi-mode optical microcavity, *Phys. Rev. A* **98**, 013854 (2018).
- [13] M. Li, C.-L. Zou, C.-H. Dong, and D.-X. Dai, Optimal third-harmonic generation in an optical microcavity with  $\chi^{(2)}$  and  $\chi^{(3)}$  nonlinearities, *Opt. Express* **26**, 27294 (2018).
- [14] C. Cui, L. Zhang, and L. Fan, In situ control of effective kerr nonlinearity with pockels integrated photonics, *Nature Physics* **18**, 497 (2022).
- [15] J. Szabados, B. Sturman, and I. Breunig, Frequency comb generation threshold via second-harmonic excitation in  $\chi^{(2)}$  optical microresonators, *APL Photonics* **5** (2020).
- [16] A. Villois and D. V. Skryabin, Soliton and quasi-soliton frequency combs due to second harmonic generation in microresonators, *Opt Express* **27**, 7098 (2019).
- [17] Z. Gong, M. Li, X. Liu, Y. Xu, J. Lu, A. Bruch, J. B. Surya, C. Zou, and H. X. Tang, Photonic dissipation control for kerr soliton generation in strongly raman-active media, *Phys. Rev. Lett.* **125**, 183901 (2020).
- [18] M. Yu, Y. Okawachi, R. Cheng, C. Wang, M. Zhang, A. L. Gaeta, and M. Lončar, Raman lasing and soliton mode-locking in lithium niobate microresonators, *Light: Science & Applications* **9**, 9 (2020).
- [19] Y. Okawachi, M. Yu, V. Venkataraman, P. M. Latawiec, A. G. Griffith, M. Lipson, M. Lončar, and A. L. Gaeta, Competition between raman and kerr effects in microresonator comb generation, *Optics Letters* **42**, 2786 (2017).
- [20] Y. Bai, M. Zhang, Q. Shi, S. Ding, Y. Qin, Z. Xie, X. Jiang, and M. Xiao, Brillouin-kerr soliton frequency combs in an optical microresonator, *Physical Review Letters* **126**, 063901 (2021).
- [21] H. Zhang, T. Tan, H.-J. Chen, Y. Yu, W. Wang, B. Chang, Y. Liang, Y. Guo, H. Zhou, H. Xia *et al.*, Soliton microcombs multiplexing using intracavity-stimulated brillouin lasers, *Physical Review Letters* **130**, 153802 (2023).
- [22] J.-Q. Wang, Y.-H. Yang, M. Li, H. Zhou, X.-B. Xu, J.-Z. Zhang, C.-H. Dong, G.-C. Guo, and C.-L. Zou, Synthetic five-wave mixing in an integrated microcavity for visible-telecom entanglement generation, *Nature Communications* **13**, 6223 (2022).
- [23] J. Szabados, D. N. Puzyrev, Y. Minet, L. Reis, K. Buse, A. Villois, D. V. Skryabin, and I. Breunig, Frequency comb generation via cascaded second-order nonlinearities in microresonators, *Physical Review Letters* **124**, 203902 (2020).
- [24] A. W. Bruch, X. Liu, Z. Gong, J. B. Surya, M. Li, C.-L. Zou, and H. X. Tang, Pockels soliton microcomb, *Nature Photonics* **15**, 21 (2021).
- [25] N. Englebert, F. De Lucia, P. Parra-Rivas, C. M. Arabí, P.-J. Sazio, S.-P. Gorza, and F. Leo, Parametrically driven kerr cavity solitons, *Nature Photonics* **15**, 857 (2021).
- [26] M. Li, X.-X. Xue, Y.-L. Zhang, X.-B. Xu, C.-H. Dong, G.-C. Guo, and C.-L. Zou, Breaking the efficiency limitations of dissipative kerr soliton using nonlinear couplers, *arXiv preprint arXiv:2203.08453* (2022).
- [27] A. Lukashchuk, J. Riemensberger, A. Tusnín, J. Liu, and T. J. Kippenberg, Chaotic microcomb-based parallel ranging, *Nature Photonics* pp. 1–8 (2023).
- [28] Y. Hu, M. Yu, B. Buscaino, N. Sinclair, D. Zhu, R. Cheng, A. Shams-Ansari, L. Shao, M. Zhang, J. M. Kahn *et al.*, High-efficiency and broadband on-chip electro-optic frequency comb generators, *Nature Photonics* **16**, 679 (2022).
- [29] M. Yu, D. Barton III, R. Cheng, C. Reimer, P. Kharel, L. He, L. Shao, D. Zhu, Y. Hu, H. R. Grant *et al.*, Integrated femtosecond pulse generator on thin-film lithium niobate, *Nature* **612**, 252 (2022).
- [30] B. Yao, S.-W. Huang, Y. Liu, A. K. Vinod, C. Choi, M. Hoff, Y. Li, M. Yu, Z. Feng, D.-L. Kwong *et al.*, Gate-tunable frequency combs in graphene-nitride microresonators, *Nature* **558**, 410 (2018).
- [31] K. Sasagawa and M. Tsuchiya, Highly efficient third harmonic generation in a periodically poled mgo: Linbo3 disk resonator, *Applied Physics Express* **2**, 122401 (2009).
- [32] R. Wolf, I. Breunig, H. Zappe, and K. Buse, Cascaded second-order optical nonlinearities in on-chip micro rings, *Optics express* **25**, 29927 (2017).
- [33] S. Liu, Y. Zheng, and X. Chen, Cascading second-order nonlinear processes in a lithium niobate-on-insulator microdisk, *Optics letters* **42**, 3626 (2017).
- [34] J. S. Levy, M. A. Foster, A. L. Gaeta, and M. Lipson, Harmonic generation in silicon nitride ring resonators, *Optics express* **19**, 11415 (2011).
- [35] M. A. Guidry, D. M. Lukin, K. Y. Yang, R. Trivedi, and J. Vučković, Quantum optics of soliton microcombs, *Nature Photonics* **16**, 52 (2022).
- [36] H.-t. Tan and H. Huang, Bright quadripartite entanglement from competing  $\chi^{(2)}$  nonlinearities, *Physical Review A* **83**, 015802 (2011).
- [37] Z. Yang, M. Jahanbozorgi, D. Jeong, S. Sun, O. Pfister, H. Lee, and X. Yi, A squeezed quantum microcomb on a chip, *Nature Communications* **12**, 4781 (2021).
- [38] M. Kues, C. Reimer, J. M. Lukens, W. J. Munro, A. M. Weiner, D. J. Moss, and R. Morandotti, Quantum optical microcombs, *Nature Photonics* **13**, 170 (2019).
- [39] M. A. Marte, Competing nonlinearities, *Physical Review A* **49**, R3166 (1994).
- [40] A. Gordon and B. Fischer, Phase transition theory of many-mode ordering and pulse formation in lasers, *Physical review letters* **89**, 103901 (2002).
- [41] C. Ropp, N. Bachelard, D. Barth, Y. Wang, and X. Zhang, Dissipative self-organization in optical space, *Nature Photonics* **12**, 739 (2018).
- [42] N. M. Kondratiev, V. E. Lobanov, A. E. Shitikov, R. R. Galiev, D. A. Chermoshentsev, N. Y. Dmitriev, A. N. Danilin, E. A. Lonshakov, K. N. Min'kov, D. M. Sokol *et al.*, Recent advances in laser self-injection locking to high- $q$  microresonators, *arXiv preprint arXiv:2212.05730* (2022).
- [43] A. Roy, R. Nehra, C. Langrock, M. Fejer, and A. Marandi, Non-equilibrium phase transitions in coupled nonlinear optical resonators, *arXiv preprint arXiv:2205.01344* (2022).
- [44] T. J. Kippenberg, A. L. Gaeta, M. Lipson, and M. L. Gorodetsky, Dissipative kerr solitons in optical microresonators, *Science* **361**, eaan8083 (2018).
- [45] Z. Lu, H.-J. Chen, W. Wang, L. Yao, Y. Wang, Y. Yu, B. Little, S. Chu, Q. Gong, W. Zhao *et al.*, Synthesized soliton crystals, *Nature communications* **12**, 3179 (2021).
- [46] G. Moille, L. Chang, W. Xie, A. Rao, X. Lu, M. Davanco, J. E. Bowers, and K. Srinivasan, Dissipative kerr solitons in a iii-v microresonator, *Laser & Photonics Reviews* **14**, 2000022 (2020).
- [47] P. Del'Haye, O. Arcizet, A. Schliesser, R. Holzwarth, and T. J. Kippenberg, Full stabilization of a microresonator-based optical frequency comb, *Physical Review Letters* **101**, 053903 (2008).
- [48] Q.-F. Yang, B. Shen, H. Wang, M. Tran, Z. Zhang, K. Y. Yang, L. Wu, C. Bao, J. Bowers, A. Yariv *et al.*, Vernier spectrometer using counterpropagating soliton microcombs, *Science* **363**, 965 (2019).
- [49] V. Brasch, E. Lucas, J. D. Jost, M. Geiselmann, and T. J. Kippenberg, Self-referenced photonic chip soliton kerr frequency comb, *Light: Science & Applications* **6**, e16202 (2017).

- [50] Z. L. Newman, V. Maurice, T. Drake, J. R. Stone, T. C. Briles, D. T. Spencer, C. Fredrick, Q. Li, D. Westly, B. R. Ilic *et al.*, Architecture for the photonic integration of an optical atomic clock, *Optica* **6**, 680 (2019).
- [51] R. Niu, M. Li, S. Wan, Y. R. Sun, S.-M. Hu, C.-L. Zou, G.-C. Guo, and C.-H. Dong, khz-precision wavemeter based on reconfigurable microsoliton, *Nature Communications* **14**, 169 (2023).
- [52] Q.-F. Yang, Q.-X. Ji, L. Wu, B. Shen, H. Wang, C. Bao, Z. Yuan, and K. Vahala, Dispersive-wave induced noise limits in miniature soliton microwave sources, *Nature communications* **12**, 1442 (2021).
- [53] J. Lu, M. Li, C.-L. Zou, A. A. Sayem, and H. X. Tang, Toward 1% single-photon anharmonicity with periodically poled lithium niobate microring resonators, *Optica* **7**, 1654 (2020).
- [54] G. Marty, S. Combri , F. Raineri, and A. De Rossi, Photonic crystal optical parametric oscillator, *Nature photonics* **15**, 53 (2021).
- [55] M. Zhao and K. Fang, Ingap quantum nanophotonic integrated circuits with 1.5% nonlinearity-to-loss ratio, *Optica* **9**, 258 (2022).
- [56] J. Lin, N. Yao, Z. Hao, J. Zhang, W. Mao, M. Wang, W. Chu, R. Wu, Z. Fang, L. Qiao, W. Fang, F. Bo, and Y. Cheng, Broadband quasi-phase-matched harmonic generation in an on-chip monocrystalline lithium niobate microdisk resonator, *Phys. Rev. Lett.* **122**, 173903 (2019).
- [57] Supplementary material for "autonomous frequency locking for zero-offset frequency comb".
- [58] X. Lu, Q. Li, D. A. Westly, G. Moille, A. Singh, V. Anant, and K. Srinivasan, Chip-integrated visible–telecom entangled photon pair source for quantum communication, *Nature physics* **15**, 373 (2019).
- [59] L. Ledezma, A. Roy, L. Costa, R. Sekine, R. Gray, Q. Guo, R. Nehra, R. M. Briggs, and A. Marandi, Octave-spanning tunable infrared parametric oscillators in nanophotonics, *Science Advances* **9**, eadf9711 (2023).
- [60] E. X. DeJesus and C. Kaufman, Routh-hurwitz criterion in the examination of eigenvalues of a system of nonlinear ordinary differential equations, *Physical Review A* **35**, 5288 (1987).
- [61] K. Hitachi, A. Ishizawa, T. Nishikawa, M. Asobe, and T. Sogawa, Carrier-envelope offset locking with a 2f-to-3f self-referencing interferometer using a dual-pitch ppln ridge waveguide, *Optics Express* **22**, 1629 (2014).
- [62] X. Liu, Z. Gong, A. W. Bruch, J. B. Surya, J. Lu, and H. X. Tang, Aluminum nitride nanophotonics for beyond-octave soliton microcomb generation and self-referencing, *Nature communications* **12**, 1 (2021).
- [63] H.-J. Chen, Q.-X. Ji, H. Wang, Q.-F. Yang, Q.-T. Cao, Q. Gong, X. Yi, and Y.-F. Xiao, Chaos-assisted two-octave-spanning microcombs, *Nature communications* **11**, 2336 (2020).
- [64] T. Herr, V. Brasch, J. D. Jost, C. Y. Wang, N. M. Kondratiev, M. L. Gorodetsky, and T. J. Kippenberg, Temporal solitons in optical microresonators, *Nature Photonics* **8**, 145 (2014).
- [65] D. V. Skryabin, Coupled-mode theory for microresonators with quadratic nonlinearity, *JOSA B* **37**, 2604 (2020).
- [66] Z. Ye, H. Jia, Z. Huang, C. Shen, J. Long, B. Shi, Y.-H. Luo, L. Gao, W. Sun, H. Guo *et al.*, Foundry manufacturing of tight-confinement, dispersion-engineered, ultralow-loss silicon nitride photonic integrated circuits, *Photonics Research* **11**, 558 (2023).
- [67] E. Timurdogan, C. V. Poulton, M. J. Byrd, and M. R. Watts, Electric field-induced second-order nonlinear optical effects in silicon waveguides, *Nature Photonics* **11**, 200 (2017).
- [68] X. Lu, G. Moille, A. Rao, D. A. Westly, and K. Srinivasan, Efficient photoinduced second-harmonic generation in silicon nitride photonics, *Nature Photonics* **15**, 131 (2021).

# SUPPLEMENTARY MATERIAL for ‘‘Autonomous frequency locking for zero-offset microcomb’’

## I. DERIVATION OF THE OPO LASER FREQUENCY

We consider the OPO process based on degenerate four-wave mixing among photonic modes  $a, b, c$ , which can be modeled by the Hamiltonian

$$H = \omega_a a^\dagger a + \omega_b b^\dagger b + \omega_c c^\dagger c + g_3 (abc^{\dagger 2} + a^\dagger b^\dagger c^2) + i\varepsilon_p (c^\dagger e^{-i\omega_p t} + c e^{i\omega_p t}). \quad (\text{S.1})$$

$\omega_{a,b,c}$  denotes the resonant frequency of the corresponding mode and  $\omega_{a,b}$  are close to  $\frac{2}{3}\omega_p$  and  $\frac{4}{3}\omega_p$ , respectively.  $g_3$  is the nonlinear coupling rate,  $\varepsilon_p$  and  $\omega_p$  are the driving strength and frequency on mode  $c$ , respectively. When operation below the threshold, the photon amplitudes in mode  $a, b$  are much weaker than that in the pump mode  $c$  and the field in mode  $c$  can be approximated to be  $\gamma = \frac{\varepsilon_p}{-i(\omega_c - \omega_p) - \kappa_c}$ , with  $\kappa_c$  being the dissipation rate of the mode. Then, in the symmetric rotating frame of  $\frac{2}{3}\omega_p a^\dagger a + \frac{4}{3}\omega_p b^\dagger b$ , the Hamiltonian reduces to

$$H = \Delta_a a^\dagger a + \Delta_b b^\dagger b + g_{\text{eff}} (ab + a^\dagger b^\dagger), \quad (\text{S.2})$$

where  $g_{\text{eff}} = g_3 |\gamma|^2$ . The dynamics of the operators can be derived according to the Heisenberg-Langevin

$$\frac{d}{dt} a = (-i\Delta_a - \kappa_a) a - ig_{\text{eff}} b^\dagger + \sqrt{2\kappa_a} a_{in}, \quad (\text{S.3})$$

$$\frac{d}{dt} b = (-i\Delta_b - \kappa_b) b - ig_{\text{eff}} a^\dagger + \sqrt{2\kappa_b} b_{in}. \quad (\text{S.4})$$

$a_{in}$  and  $b_{in}$  are the input noise on the photonic modes. Introducing the Fourier transform

$$O(\omega) = \frac{1}{2\pi} \int O(t) e^{i\omega t} dt, \quad (\text{S.5})$$

$$O^\dagger(-\omega) = \frac{1}{2\pi} \int O^\dagger(t) e^{i\omega t} dt, \quad (\text{S.6})$$

the dynamical equations transform to

$$0 = [-i(\Delta_a + \omega) - \kappa_a] a(\omega) - ig_{\text{eff}} b^\dagger(-\omega) + \sqrt{2\kappa_a} a_{in}(\omega), \quad (\text{S.7})$$

$$0 = [i(\Delta_a - \omega) - \kappa_a] a^\dagger(-\omega) + ig_{\text{eff}} b(\omega) + \sqrt{2\kappa_a} a_{in}^\dagger(-\omega), \quad (\text{S.8})$$

$$0 = [-i(\Delta_b + \omega) - \kappa_b] b(\omega) - ig_{\text{eff}} a^\dagger(-\omega) + \sqrt{2\kappa_b} b_{in}(\omega), \quad (\text{S.9})$$

$$0 = [i(\Delta_b - \omega) - \kappa_b] b^\dagger(-\omega) + ig_{\text{eff}} a(\omega) + \sqrt{2\kappa_b} b_{in}^\dagger(-\omega). \quad (\text{S.10})$$

In a compact form

$$\begin{bmatrix} \Gamma_a^+ & 0 & 0 & -ig_3 |\gamma|^2 \\ 0 & \Gamma_a^- & ig_3 |\gamma|^2 & 0 \\ 0 & -ig_3 |\gamma|^2 & \Gamma_b^+ & 0 \\ ig_3 |\gamma|^2 & 0 & 0 & \Gamma_b^- \end{bmatrix} \begin{bmatrix} a(\omega) \\ a^\dagger(-\omega) \\ b(\omega) \\ b^\dagger(-\omega) \end{bmatrix} + \begin{bmatrix} \sqrt{2\kappa_a} a_{in}(\omega) \\ \sqrt{2\kappa_a} a_{in}^\dagger(-\omega) \\ \sqrt{2\kappa_b} b_{in}(\omega) \\ \sqrt{2\kappa_b} b_{in}^\dagger(-\omega) \end{bmatrix} = 0, \quad (\text{S.11})$$

where  $\Gamma_a^\pm = \mp i(\Delta_a \pm \omega) - \kappa_a$  and  $\Gamma_b^\pm = \mp i(\Delta_b \pm \omega) - \kappa_b$ . The solution is

$$\begin{bmatrix} a(\omega) \\ a^\dagger(-\omega) \\ b(\omega) \\ b^\dagger(-\omega) \end{bmatrix} = [M(\omega)]_{4 \times 4} \begin{bmatrix} \sqrt{2\kappa_a} a_{in}(\omega) \\ \sqrt{2\kappa_a} a_{in}^\dagger(-\omega) \\ \sqrt{2\kappa_b} b_{in}(\omega) \\ \sqrt{2\kappa_b} b_{in}^\dagger(-\omega) \end{bmatrix}. \quad (\text{S.12})$$



The power spectral

$$\begin{aligned} S_a(\omega) &= \langle a^\dagger(\omega) a(\omega) \rangle \\ &= \frac{\kappa_a}{\pi} |M_{12}|^2 + \frac{\kappa_b}{\pi} |M_{14}|^2, \end{aligned} \quad (\text{S.13})$$

where we have used the property of the quantum noise

$$\langle O_{in,i}^\dagger(\omega) O_{in,j}(\omega') \rangle = 0, \quad (\text{S.14})$$

$$\langle O_{in,i}(\omega) O_{in,j}^\dagger(\omega') \rangle = \frac{1}{2\pi} \delta_{ij} \delta(\omega - \omega'), \quad (\text{S.15})$$

for  $O_{in,j} \in \{a_{in}, b_{in}\}$ . By solving the expression of  $M(\omega)$ , we find the power spectral diverges when

$$[-i(\Delta_a + \omega) - \kappa_a][i(\Delta_b - \omega) - \kappa_b] = g_3^2 |\gamma^4|. \quad (\text{S.16})$$

It corresponds to the laser threshold of the OPO process. We can solve this equation to obtain the root of  $\omega$  as the laser frequency of mode  $a$  respect to the frame  $\frac{2}{3}\omega_p$

$$\delta_s = \frac{\Delta_b \kappa_a - \Delta_a \kappa_b}{\kappa_a + \kappa_b}, \quad (\text{S.17})$$

which depends on the mode detuning and dissipation.

## II. CONDITION OF AUTONOMOUS-LOCKING

For the cascaded OPO-SHG system with resonant drive on mode  $c$ , the Hamiltonian in the rotating frame reads,

$$H = \Delta_a a^\dagger a + \Delta_b b^\dagger b + g_3 (abc^{\dagger 2} + a^\dagger b^\dagger c^2) + g_2 (a^2 b^\dagger + a^{\dagger 2} b) + i\varepsilon_p (c^\dagger - c). \quad (\text{S.18})$$

When operation above the threshold, the optical fields in mode  $\{a, b, c\}$  can be treated as complex numbers  $\{\alpha, \beta, \gamma\}$  for  $g_{2,3}$  much smaller than the mode dissipation. The dynamics of the system follows

$$\frac{d}{dt} \alpha = (-i\Delta_a - \kappa_a) \alpha - ig_3 \beta^* \gamma^2 - 2ig_2 \alpha^* \beta \quad (\text{S.19})$$

$$\frac{d}{dt} \beta = (-i\Delta_b - \kappa_b) \beta - ig_3 \alpha^* \gamma^2 - ig_2 \alpha^2 \quad (\text{S.20})$$

$$\frac{d}{dt} \gamma = -\kappa_c c - 2ig_3 \gamma^* \alpha \beta + \varepsilon_p. \quad (\text{S.21})$$

Since the phase of  $\gamma$  can be tuned by the drive field  $\varepsilon_p$ , we treat  $\gamma$  as a real number in the following derivations. From Eq. S.20, we get

$$\gamma^2 = \frac{(-i\Delta_b - \kappa_b) \beta - ig_2 \alpha^2}{ig_3 \alpha^*}. \quad (\text{S.22})$$

Submit it into Eq.S.19, we get

$$\begin{aligned} 0 &= (-i\Delta_a - \kappa_a) \alpha - ig_3 \beta^* \frac{(-i\Delta_b - \kappa_b) \beta - ig_2 \alpha^2}{ig_3 \alpha^*} - 2ig_2 \alpha^* \beta \\ &= (-i\Delta_a - \kappa_a) \alpha - \beta^* \frac{(-i\Delta_b - \kappa_b) \beta - ig_2 \alpha^2}{\alpha^*} - 2ig_2 a^\dagger b \end{aligned} \quad (\text{S.23})$$

Then

$$0 = (-i\Delta_a - \kappa_a) |\alpha|^2 - \beta^* [(-i\Delta_b - \kappa_b) \beta - ig_2 \alpha^2] - 2ig_2 \alpha^* \beta \quad (\text{S.24})$$

$$= (-i\Delta_a - \kappa_a) |\alpha|^2 - (-i\Delta_b - \kappa_b) |\beta|^2 + ig_2 \alpha^2 \beta^* - 2ig_2 \alpha^* \beta. \quad (\text{S.25})$$

Denote  $b = x + iy$ , these equations can be split to real and imaginary parts,

$$3g_2\alpha^2 y + \kappa_b x^2 + \kappa_b y^2 - \kappa\alpha^2 = 0 \quad (\text{S.26})$$

$$-g_2\alpha^2 x + \Delta_b x^2 + \Delta_b y^2 - \Delta_a\alpha^2 = 0. \quad (\text{S.27})$$

The roots of the equation is

$$x = \frac{1}{2g_2^2(9\Delta_b^2 + \kappa_b^2)} \left[ 9g_2^3\Delta_b\alpha^2 + 2g_2\kappa_b(\Delta_b\kappa_a - \Delta_a\kappa_b) \mp 3\sqrt{g_2^2\Delta_b^2(9g_2^4\alpha^4 - 4(\Delta_b\kappa_a - \Delta_a\kappa_b)^2 + 4g_2^2\alpha^2(9\Delta_a\Delta_b + \kappa_a\kappa_b))} \right], \quad (\text{S.28})$$

$$y = \pm \frac{1}{2g_2^2\Delta_b(9\Delta_b^2 + \kappa_b^2)} \left[ -3g_2^3\Delta_b\kappa_b\alpha^2 + 6g_2\Delta_b^2(\Delta_b\kappa_a - \Delta_a\kappa_b) + 3\sqrt{g_2^2\Delta_b^2(9g_2^4\alpha^4 - 4(\Delta_b\kappa_a - \Delta_a\kappa_b)^2 + 4g_2^2\alpha^2(9\Delta_a\Delta_b + \kappa_a\kappa_b))} \right]. \quad (\text{S.29})$$

For the simple case where  $\kappa_a = \kappa_b$ , it can be seen that

$$9g_2^4\alpha^4 - 4(\Delta_a - \Delta_b)^2\kappa^2 + 4g_2^2\alpha^2(9\Delta_a\Delta_b + \kappa^2) \geq 0 \quad (\text{S.30})$$

is required for real roots of  $x$  and  $y$ , i.e., a stable solution of the system or a self-locked state. For small detuning  $\Delta_{a,b} \ll \kappa$ , the condition reduces to

$$g_2^2\alpha^2 \geq (\Delta_a - \Delta_b)^2. \quad (\text{S.31})$$

### III. COMB SIMULATION

The frequency comb evolution is described by coupling mode equations (CME)

$$\frac{da_j}{dt} = (-i\Delta_j - \kappa_j)a_j - i\Sigma 2g_{ikln}^{(3)}a_k^\dagger a_l a_n - i\varepsilon_p \delta_{jp}, \quad (\text{S.32})$$

where  $\Delta_j = \omega_j - (\omega_p + \omega_{\text{rep,rot}} \cdot j)$ ,  $\omega_j$  is the frequency of cold resonance,  $\omega_{\text{rep,rot}}$  is the frequency interval of rotation frame. In order to simulate how  $\chi^{(2)}$  interaction perturb the kerr soliton comb, we start from pure kerr soliton then turn on  $\chi^{(2)}$  coupling for targeted fundamental mode  $f$  and second harmonic mode  $s$ . The pure kerr soliton is simulated in trivial rotating frame where  $\omega_{\text{rep,rot}}$  equals to the nominal repetition rate  $\omega_{\text{rep}}$  of frequency comb. General parameter in LN ring resonator are used for simulation, as shown in Fig. S1 (a). After kerr soliton is ready, we further prepare soliton samples with different photon number in modes  $f, s$  by tuning the local integrated dispersion  $\Delta_f$  and  $\Delta_s$ , which mimic dispersive waves in real experiment, as shown in Fig. S1 (b-i). After changing Dint for modes  $f$  and  $s$ , the initial kerr soliton keeps evolution until reaching a new stable state to make sure there is no internal oscillation in the system, as shown in Fig. S1 (b-ii). These samples can be used to investigate how locking range  $f_{\text{ceo}}$  is influenced by photon number in  $f$  and  $s$  modes, relative results are presented in Fig. 4 of main text.

We choose modes with relative index  $\mu_f = -180$  and  $\mu_s = +180$  as  $f$  and  $s$  mode, respectively. Therefore, absolute pump mode number  $m_p = \mu_s - 2\mu_f = 540$ . The CME including  $\chi^{(2)}$  coupling for  $f$  and  $s$  modes are

$$\frac{da_f}{dt} = (-i\Delta'_f - \kappa_f)a_f - i\Sigma 2g_{ikln}^{(3)}a_k^\dagger a_l a_n - ig^{(2)}a_f^\dagger a_s - i\varepsilon_p \delta_{fp}, \quad (\text{S.33})$$

$$\frac{da_s}{dt} = (-i\Delta'_s - \kappa_s)a_s - i\Sigma 2g_{ikln}^{(3)}a_k^\dagger a_l a_n - ig^{(2)}a_f^\dagger a_s - i\varepsilon_p \delta_{sp}. \quad (\text{S.34})$$

In order to determine whether soliton reaches locked state with  $f_{\text{ceo}} = 0$  after turning on  $\chi^{(2)}$ , we simulate its evolution by switching to  $f_{\text{ceo}}$ -free frame where  $\omega_{\text{rep,rot}} = \omega_p/m_p$ . Here  $\omega_p$  is pump frequency after pure kerr soliton formation and won't be swept anymore in later simulation. We assign kerr soliton samples with an initial  $f_{\text{ceo}}$  by setting its repetition rate be  $\omega_{\text{rep}} = (\omega_p - f_{\text{ceo}})/m_p$ , hence  $\Delta'_j$  in the new rotating frame is written as

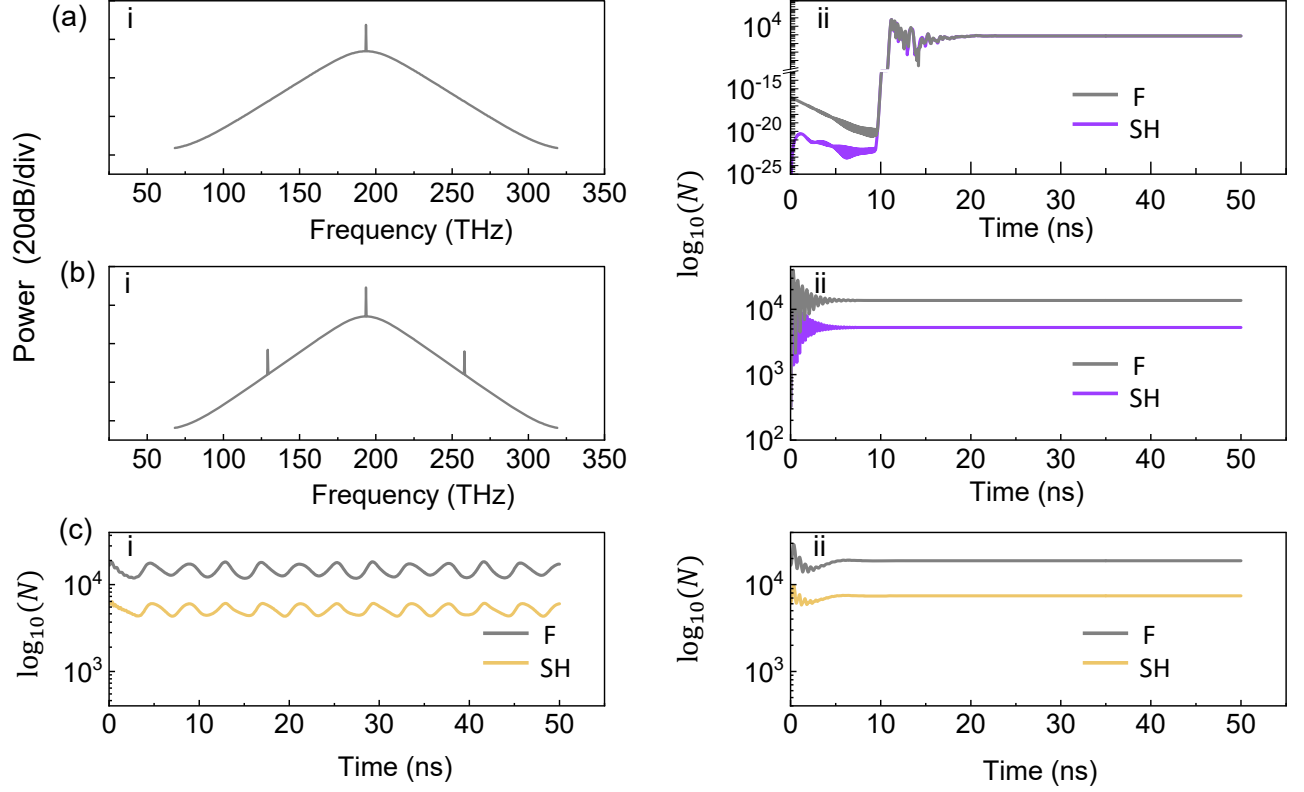


**Fig S1.** (a) i: Initial pure kerr soliton. ii: Evolution of photon number in modes  $f$  and  $s$  during soliton formation. (b) i: Decreasing Dint of modes  $f$  and  $s$  by a factor of 6.4 and 4, respectively, which results in enhanced photon number in these two modes. ii: photon number evolution after changing Dint. (c) Set initial  $f_{\text{ceo}}$  to be  $3\kappa$ , i: Add  $\chi^{(2)}$  coupling between modes  $f$  and  $s$  with  $g_2 = 1.2\text{MHz}$ . ii: with  $g_2 = 2.4\text{MHz}$ . All simulation share the following parameters:  $g_3 = 0.55\text{Hz}$ ,  $\kappa = 94.89\text{MHz}$ ,  $D_2 = 0.67\text{MHz}$ ,  $P_{\text{pump}} = 0.25\text{W}$ .

$$\Delta'_j = \omega_0 + \omega_{\text{rep}} \cdot j + \frac{D_2}{2!} \cdot j^2 + \frac{D_3}{3!} \cdot j^3 - (\omega_p + \omega_{\text{rep,rot}} \cdot j). \quad (\text{S.35})$$

The criterion for locking is that the photon number of all modes can finally reaches steady-state after evolving in this new  $f_{\text{ceo}}$ -free frame with  $\chi^{(2)}$  terms added in.

In practical experiments, once the phase-matching of SHG between mode  $f$  to mode  $s$  is designed, SFG/DFG between mode pairs near  $f$ ,  $s$  also take place simultaneously, which contribute to self-locking of zero- $f_{\text{ceo}}$  comb. Due to cavity dispersion, the  $\chi^{(2)}$  interaction has a finite bandwidth and SFG is only effective for several mode-pairs near mode  $f$ . According to the numerical results shown in Fig. S2, the system has a larger locking range when more modes are involved in  $\chi^{(2)}$  interaction. Therefore, it is preferred to engineer a flat dispersion for broadband  $\chi^{(2)}$  interaction as well as for broadband comb generation.

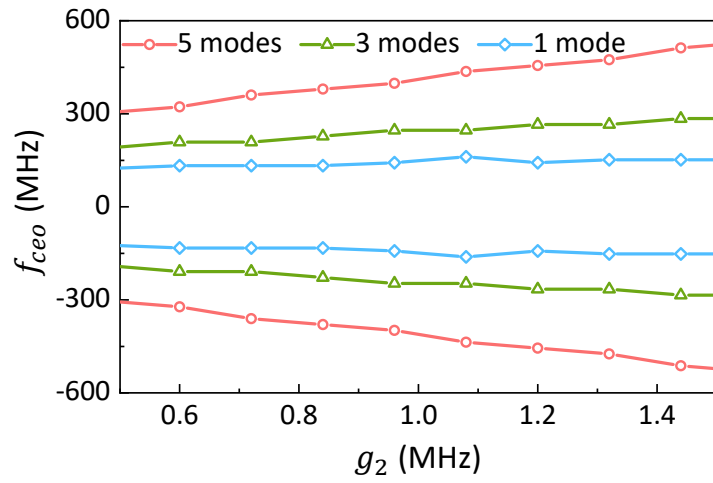


**Fig S2.** Locking range  $f_{ceo}$  changes with  $\chi^{(2)}$  coupling strength  $g_2$  with different mode pairs participating in  $\chi^{(2)}$  process. Negative  $f_{ceo}$  means the actual  $f_{ceo}$  is close to  $f_{rep}$ .